AAS 07-103

Absolute and Relative Position Determination Using Variable Celestial X-ray Sources

Suneel I. Sheikh
(ASTER Labs, Inc.)
A. Robert Golshan
(Johns Hopkins University Applied Physics Laboratory)
and
Darryll J. Pines
(University of Maryland)

30th ANNUAL AAS GUIDANCE AND CONTROL CONFERENCE

February 3-7, 2007
Breckenridge, Colorado

Sponsored by
Rocky Mountain Section

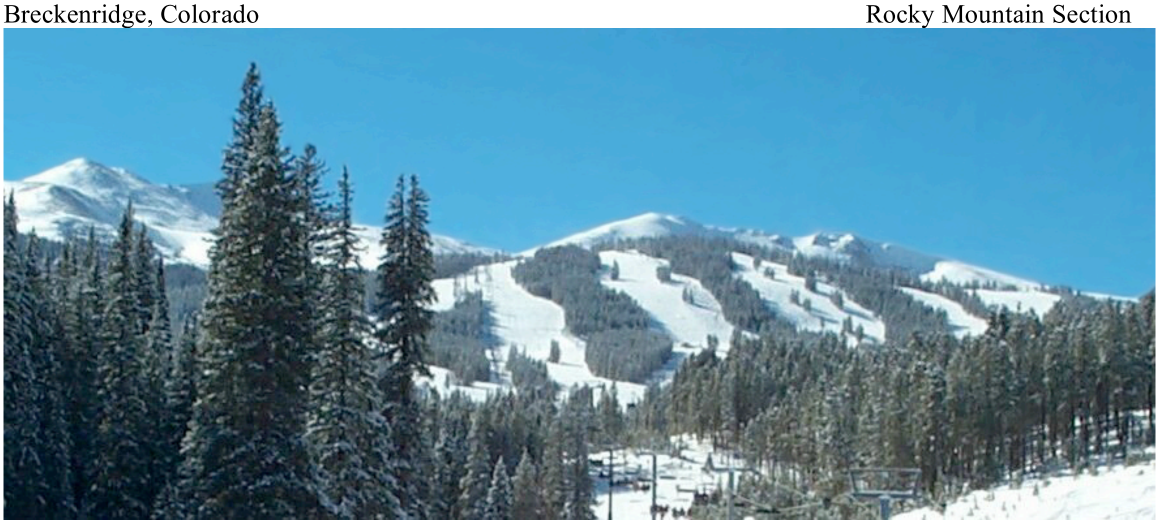

AAS Publications Office, P.O. Box 28130 - San Diego, California 92198

AAS 07–103

ABSOLUTE AND RELATIVE POSITION DETERMINATION USING VARIABLE CELESTIAL X-RAY SOURCES

Suneel I. Sheikh†, A. Robert Golshan◊, and Darryll J. Pines§

This paper presents techniques for determining spacecraft position using variable celestial sources, including pulsars, which emit X-ray radiation. These bright sources produce unique and periodic signals that can be tracked given sufficient observation duration. Utilizing the known frequency of these signals, the combination of signals from multiple sources can be utilized to resolve the ambiguous integer number of cycles between the spacecraft and a reference origin. Methods are provided to analyze the signals using a maximum-likelihood estimator for both actual and simulated source data. Cycle resolution techniques are presented as well as representative performance for Earth-orbiting spacecraft with simulated data. Position is determined with respect to the origin of an absolute reference frame or relative to another reference point in space.

INTRODUCTION

Determining the *absolute* position of a spacecraft is an important function of its mission operations. Spacecraft that can generate autonomous absolute position solutions have increased functionality over vehicles that must rely upon transmitted solutions. Accurate position knowledge ensures the vehicle is following its intended path, allows the vehicle to safely control itself around potential obstacles, and most importantly assists the vehicle in pursuing its intended goals. Alternatively, techniques that produce spacecraft position solutions *relative* to other vehicles or planetary bodies that are typically in motion themselves allow the spacecraft to safely and reliably operate within the close proximity to these objects.

Various methods exist to solve for the absolute position of a spacecraft. These include orbit determination based upon measurements from Earth-based observation stations in either the optical or radio band; vehicle tracking using the NASA Deep Space Network (DSN) [1]; and occultation of celestial objects [2]. Increased use of the Global Position System (GPS) and other Global Navigation Satellite Systems (GNSS) have demonstrated significant utility for spacecraft navigation [3, 4]. However, limitations exist for GNSS systems, including limited signal visibility, availability, and low signal strength. GNSS systems only operate only near-Earth, thus for applications far from Earth, alternate methods must be utilized.

To augment existing space navigation systems, it has been proposed to employ variable celestial sources [5-12]. In order to utilize the variable celestial sources for absolute position determination, the

† Chief Research Scientist, ASTER Labs, Inc., 5005 Kenesaw St., College Park, Maryland 20740. Email: sheikh@asterlabs.com. Phone: 301-982-7430, FAX: 301-982-7438. Web site: www.asterlabs.com.

◊ Senior Professional Staff, Johns Hopkins University Applied Physics Laboratory, 11100 Johns Hopkins Road, Laurel, MD 20723. Email: robert.golshan@jhuapl.edu. Phone: 240-228-2795, FAX: 240-228-6635. Web site: www.jhuapl.edu.

§ Department Chairman, Aerospace Engineering, Room 3154 Martin Hall, University of Maryland, College Park, Maryland 20742. Email: pines@umd.edu. Phone: 301-405-0263, FAX: 301-314-9001. Web site: www.enae.umd.edu.

specific pulse cycle received from a source must be identified. This paper provides methods to demonstrate how the unknown, or *ambiguous*, number of pulse cycles can be resolved, such that the absolute position of a spacecraft can be produced with respect to a chosen reference frame origin. An important attribute of these methods is they are applicable to all regions of space, including throughout the solar system, as well as further into the Milky Way galaxy, and perhaps beyond. The determination of unknown cycles for variable celestial sources, or *pulse phase cycle ambiguity resolution* process, is in some manner similar to the methods used in GNSS navigation systems, including particularly those used for surveying and differential positioning systems. However, the ambiguity resolution process for variable celestial sources is unique in many ways from the GNSS systems, as listed in Table 1. The absolute and relative navigation processes considered in this text are different from those that compute integrated vehicle motion using *a priori* navigation information. Those processes use continuous estimates of navigation values, and new measurements are recursively utilized to compute accurate position and velocity solutions [9, 13].

Table 1
COMPARISON OF GNSS AND PULSAR AMBIGUITY RESOLUTION PROCESSES

Attribute	Comparison Description
Antennas vs. Models	GNSS systems use multiple antennas to determine cycle ambiguities measured between the antenna locations. Pulsar-based systems would primarily use the measured pulse arrival at a detector and compare this to the expected arrival time produced by a model at another location. A relative positioning system, however, may be able to use multiple detectors at different locations to determine the offset of each detector relative to one another.
Multiple Wavelengths	A pulsar-based navigation system can use the different emitted wavelengths of these sources, anywhere from radio through gamma-ray bands. Different pulse detection methods and hardware may be required in different wavelength bands.
Different Frequencies	GNSS systems currently use one or a few frequencies to complete its ambiguity resolution process. Each pulsar has a unique signature, thus each cycle period can be quite different. These many different pulse cycle lengths can assist the cycle ambiguity resolution process.
Range Measurements	GNSS methods make use of direct range measurements between an orbiting satellite and receiving antennas using accurate data time tagging. Celestial sources are very distant from the solar system. These sources do not provide time information with their signal and, since their distances are not known sufficiently accurate, no direct range measurement can be made from them.
Signal Pulse	The GNSS cycles are determined from the radio carrier wave combined with the code signal. Pulsars emit pulses directly at a specified frequency. Although the carrier signal from pulsars could be monitored, the pulse cycles themselves are used in the ambiguity resolution process.
Doppler Effects	GNSS receivers can accurately track the carrier wave of the signal transmitted from the orbiting satellites. Thus, measurements of carrier phase rate can be used in GNSS cycle ambiguity resolution. The cycle phase rate is typically not measured from pulsars; however, the observed Doppler effect is may potentially be determined as the detector is in motion.
Availability & Control	GNSS systems are developed and maintained by humans. Celestial sources have been developed and maintained by the Universe. Although control of these sources is unavailable, their immense distance and significant signal strength allow them to provide usable signals throughout the Milky Way galaxy and beyond.

Details of the methods and algorithms to determine the phase cycle ambiguities from pulsars are provided in this paper. The following section on *Variable Celestial X-ray Sources* provides a brief discussion of the important characteristics of these sources relevant to spacecraft navigation. The *Observables and Errors* section provides a description of quantities that are measured from variable celestial sources. Errors that can be significant in this process are also presented. The *Pulsar Phase Estimation* section describes the details of determining pulse phase from each observation and provides numerical results of this estimation process. The section on *Measurement Differences* computes all the necessary differences that are used in the proposed algorithms. The *Search Space and Cycle Ambiguity Resolution* section describes how to assemble the candidate cycle search space and then test individual candidate cycles in order to determine the most probable location for the spacecraft. Various techniques that can be implemented in this resolution process are provided. The *Relative Position* section discusses the use of these navigation techniques for applications where relative position information is required. The final section of *Numerical Simulation* discusses results of the performance of the described algorithms.

Variable Celestial X-ray Sources

Celestial sources have proven to be significant aids for navigation throughout history. A fraction of these sources are objects that emit radiation with varying levels of intensity. Subsets of these variable celestial sources are spinning neutron stars referred to as *pulsars* [14, 15]. Many pulsars rotate with remarkably stable periodicity, and the arrival time of the pulsed radiation is often predictable. Since their discovery in 1967 [16], pulsars have been found to emit throughout the radio, infrared, visible (optical), ultraviolet, X-ray, and gamma-ray energies of the electromagnetic spectrum. With their periodic radiation and wide distribution, pulsars appear to act as natural beacons, or *celestial lighthouses*, on an intergalactic scale. Since no two neutron stars are formed in exactly the same manner or have the same geometric orientation relative to Earth, the pulse frequency and shape produce a unique, identifying signature for each pulsar. Radio band emissions from these pulsars can be received in space and on Earth's surface. X-ray emissions from these sources, however, are absorbed by Earth's atmosphere, and use of this wavelength is limited to space or planetary body applications. Limiting the observation of pulsars to those that emit X-ray radiation allows for much smaller detector sizes (order of a square meter) versus radio pulsars (requiring tens of square meters of detector area).

At X-ray energy wavelengths, the primary measurable values of the emitted signal from a source are the individual high-energy photons. The rate of arrival of these photons can be measured in terms of *flux* of radiation, or number of photons per unit area per unit time. The diffuse X-ray background is an appreciably strong signal that is observed when viewing the X-ray sky, and measures of this background radiation must be considered when observing a source [17]. Variable X-ray sources must emit more radiation than this background signal in order to be detectable. Acceptable *signal-to-noise* ratios of these source signals are essentially the magnitude of the received X-ray flux above the expected X-ray background level for a location in the sky. A navigation system that utilizes pulsed emissions from pulsars would have to address the faintness, transient, flaring, bursting, and glitching aspects of these sources, as well as the presence of the diffuse X-ray background.

OBSERVABLES AND ERRORS

The diagram in Figure 1 shows the path of X-ray photon transmission from a distant emitting celestial source to a spacecraft near Earth. The vector to the source from the Sun is $\mathbf{D}$, the position of the spacecraft with respect to the Sun is $\mathbf{p}$, and the line-of-sight unit vector from the spacecraft to the source is $\hat{\mathbf{n}}_{SC}$.

An observed pulse from a celestial source is an ensemble of these photons as they arrive periodically. For a pulse arriving into the solar system to the position of the spacecraft relative to the Sun, the relationship of the transmission time, t_T, to the reception time, $t_{R_{SC}}$, is the following [9, 18],

$$\left(t_{R_{SC}} - t_T\right) = \frac{1}{c}\hat{\mathbf{n}}_{SC} \cdot \left(\mathbf{D} - \mathbf{p}\right) - \sum_{k=1}^{PB_{SS}} \frac{2GM_k}{c^3} \ln\left|\frac{\hat{\mathbf{n}}_{SC} \cdot \mathbf{p}_k + p_k}{\hat{\mathbf{n}}_{SC} \cdot \mathbf{D}_k + D_k}\right|$$
$$+ \frac{2\mu_S^2}{c^5 {D_y}^2}\left\{\begin{aligned} &\hat{\mathbf{n}}_{SC} \cdot \left(\mathbf{D} - \mathbf{p}\right)\left[\left(\frac{\left(\hat{\mathbf{n}}_{SC} \cdot \mathbf{D}\right)}{D}\right)^2 + 1\right] + 2\left(\hat{\mathbf{n}}_{SC} \cdot \mathbf{D}\right)\left(\frac{p}{D} - 1\right) \\ &+ D_y\left(\arctan\left(\frac{p_x}{D_y}\right) - \arctan\left(\frac{D_x}{D_y}\right)\right)\end{aligned}\right\} \tag{1}$$

For the discussion in this paper, the second and third terms in Eq. (1) can be combined together into a single parameter, $RelEff$, which represents all the relativistic effects along the light ray path such that,

$$\left(t_{R_{SC}} - t_T\right) = \frac{1}{c}\hat{\mathbf{n}}_{SC} \cdot \left(\mathbf{D} - \mathbf{p}\right) + \frac{1}{c} RelEff \tag{2}$$

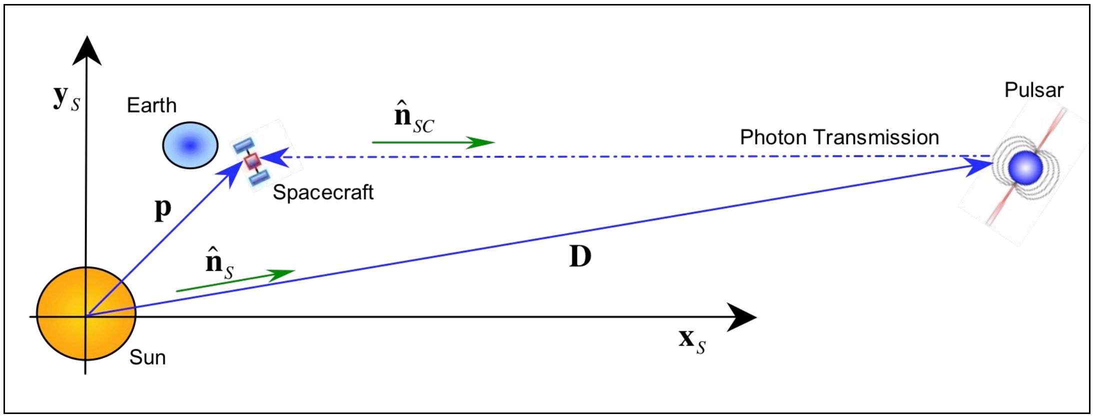

Figure 1. Light ray path arriving from distant pulsar to spacecraft within solar system.

Range Measurement

The range, ρ, from the source to the observer can be computed from the transmit and receive times of Eq. (2) as the following,

$$\rho = c\left(t_{R_{SC}} - t_T\right) = \hat{\mathbf{n}}_{SC} \cdot \left(\mathbf{D} - \mathbf{p}\right) + RelEff \tag{3}$$

Using the representation for the unit direction from the observer to the source as $\hat{\mathbf{n}}_{SC} = \left(\mathbf{D} - \mathbf{p}\right) / \left\|\mathbf{D} - \mathbf{p}\right\|$ and since vector magnitude is independent of direction, the range from Eq. (3) can be rewritten as,

$$\rho = \left\|\mathbf{D} - \mathbf{p}\right\| + RelEff = \left\|\mathbf{p} - \mathbf{D}\right\| + RelEff \tag{4}$$

Eqs. (3) and (4) represent the total path length, or range, that a pulse must travel from a source to the observer. If the observer's position, $\mathbf{p}$, and the source position vector, $\mathbf{D}$, are accurately known, then the range can be directly determined from Eq. (4). Conversely, if a range *measurement* can be computed between the source and the observer using knowledge of the source position, rearranging Eq. (3) or (4) allows a portion of the observer's position relative to the Sun to be computed. Thus any method that could provide an absolute range measurement could contribute to determining observer position.

Also from Eq. (3), if the transmission and reception times are known for an individual pulse, an absolute range measurement can be computed. However, celestial sources do not provide a means to directly determine *when* an individual pulse was transmitted. Therefore, although the reception time, t_{SC}, can be measured, the transmission time, t_T, is unknown, and the range cannot be directly determined using this expression.

Range Measurement Error

Within a navigation system, the range *measurement*, $\tilde{\rho}$, will differ from the *true* range, ρ, by some error amount, $\delta\rho$. In terms of estimated source and observer position for the i^{th} pulsar, the measured range will differ from the true range by several errors, including observer position error, $\delta\mathbf{p}$, and source position error, $\delta\mathbf{D}$, each along the direction to the source, the line-of-sight error, $\delta\tilde{\mathbf{n}}_{SC}$, relativistic effects error, $\delta RelEff$, as well as range measurement noise, η. If these errors are assumed to sum linearly with the measurement, then the true range can be represented as [9],

$$\begin{aligned}\rho_i = \tilde{\rho}_i + \delta\rho_i = \tilde{\mathbf{n}}_{SC_i} \cdot \left(\tilde{\mathbf{D}}_i - \tilde{\mathbf{p}}\right) + \widetilde{RelEff}_i + \tilde{\mathbf{n}}_{SC_i} \cdot \delta\mathbf{D}_i + \tilde{\mathbf{n}}_{SC_i} \cdot \delta\mathbf{p} \\ + \delta\tilde{\mathbf{n}}_{SC_i} \cdot \left(\tilde{\mathbf{D}}_i - \tilde{\mathbf{p}}\right) + \delta RelEff_i + \eta_i \\ = \left\|\tilde{\mathbf{p}} - \tilde{\mathbf{D}}_i\right\| + \widetilde{RelEff}_i + \left\|\delta\mathbf{p}\right\| + \left\|\delta\mathbf{D}_i\right\| + \delta RelEff_i + \eta_i\end{aligned} \quad (5)$$

Phase Measurement

A series of pulse cycles from a variable celestial source can be represented as the total cycle phase, Φ. This total cycle phase is the sum of the fraction of a pulse, ϕ, plus an integral number, N, of full integer cycles that have accumulated since a chosen initial time, as in,

$$\Phi = \phi + N \quad (6)$$

The observed phase of the i^{th} source is related to the range between the source and observer by the source pulse wavelength, λ, of the cycle, as in,

$$\rho_i = \lambda_i \Phi_i = \lambda_i \phi_i + \lambda_i N_i \quad (7)$$

From Eq. (7), if the number of cycles plus the fraction of the current pulse could be determined between the pulsar and the observer, the range can be directly computed. This equation provides an alternative method of determining range, rather than using transmit and receive times in Eq. (3) or source and receiver positions as in Eq. (4). However, since celestial sources provide no identifying information with each pulse, there is no direct method of determining which *specific* cycle is being detected at any given time.

Phase Measurement Error

The total measured cycle phase, $\tilde{\Phi}$, of a celestial source pulse within a detector system will differ from the true phase, Φ, by any phase error, $\delta\Phi$, unresolved within the system, or the measured fraction of phase, $\tilde{\phi}$, and the measured number of full cycles, $\tilde{N}$, as,

$$\Phi_i = \tilde{\Phi}_i + \delta\Phi_i = \tilde{\phi}_i + \tilde{N}_i + \delta\phi_i + \delta N_i \quad (8)$$

Since phase directly relates to range from Eq. (7), the range measurements and associated errors from Eq. (5) can be applied to the phase in Eq. (8), after the wavelength for the source has been correctly applied [9].

PULSAR PHASE ESTIMATION

In this section, the pulsar phase estimation process is addressed in more detail. This process assumes an X-ray detector onboard a spacecraft is pointed in the direction of a pulsar, which has known characteristics such as the observed flux, period, and light curve profile. For a specific observation, one or more of these characteristics may not be know precisely, in which case separate algorithms are required for real-time estimation of these parameters. For the algorithms described below, the arrival times of individual photons from the X-ray source are to be measured by the detector and used in the phase estimation process.

Signal Model

The arrival times of X-ray photons at the detector can be modeled as a Poisson point process with a periodic or quasi-periodic rate function $\Lambda(t) \geq 0$. In this representation, the number of photons arriving in a given time interval is a Poisson random variable. In other words, the probability of *k* photons arriving in the observation time interval $(t_0, t_0 + T)$ is given by the expression [19],

$$\Pr[k;(t_0, t_0 + T)] = \frac{\left\{\exp\left[-\int_{t_0}^{t_0+T} \Lambda(t)\, dt\right]\right\}\left[\int_{t_0}^{t_0+T} \Lambda(t)\, dt\right]^k}{k!}, \quad k = 0,1,2,\ldots \quad (9)$$

The rate function $\Lambda(t)$ represents the aggregate rate of all photons arriving at the detector, i.e. the sum of background and source photons. The background photons arrive at a constant rate of arrival, R_b. The source photons arrive at an average rate of R_s photons per second (ph/s) and consist of pulsed and non-pulsed photons whose ratio is dictated by the pulsed fraction parameter, $p_f \le 1$, defined as the ratio of the pulsed to total source photons. The non-pulsed source photons arrive at the constant rate of $(1-p_f)R_S$, and for all practical purposes behave the same as background photons. The pulsed source photons, on the other hand, exhibit a time-varying rate of arrival that is phase dependent. The overall rate function, therefore, consists of the following terms,

$$\Lambda(t) = R_b + (1-p_f)\,R_s + \,p_f\,R_s h\left[\phi_{\text{det}}(t)\right] \equiv \beta + \alpha h\left[\phi_{\text{det}}(t)\right] \tag{10}$$

where α and β are called the *effective source and background photon rates*, $h(\phi)$ is the *normalized pulse profile function*, and $\phi_{\text{det}}(t)$ is the observed phase at the detector. The function $h(\phi)$ is specified on the interval $\phi \in (0,1)$, but its definition is extended in the above formulation to any phase $\phi \in (-\infty,+\infty)$ by letting $h(N+\phi) = h(\phi)$ for all integers N; thus making $h(\phi)$ a periodic function with a period of one cycle. Additionally, the normalized pulse function must satisfy the conditions: $\min\limits_{\phi\in(0,1)} h(\phi) = 0$ and $\int_0^1 h(\phi)d\phi = 1$, so that it represents a rate function of a source that is entirely pulsed and has an average arrival rate of one ph/s. The observed phase at the detector can be written as,

$$\phi_{\text{det}}(t) = \theta_0 + \int_{t_0}^{t} f(t)\,dt \equiv \theta_0 + \theta(t), \qquad t \in (t_0,\, t_0 + T) \tag{11}$$

where θ_0 is the phase at the beginning of the observation interval, $f(t)$ is the observed signal frequency, and $\theta(t)$ is the phase accumulated since the beginning of the observation.

For the following analysis, in evaluating the rate function, $\Lambda(t)$, the source and background photon rates R_s and R_b were computed by multiplying their corresponding flux by an assumed detector area of 10^4 cm^2. The pulsed fraction and source flux values utilized are listed in Table 2 for the pulsars considered in this paper. A diffuse X-ray background flux was assumed fixed for all sources at a 0.0001 $ph/cm^2/s$. Normalized pulse profiles were obtained from the source references identified in the table.

Maximum-Likelihood Phase Estimation

Let $\{t_k, k = 1,2,\ldots,K\}$ denote the photon arrival times measured over the observation interval (t_0, t_0+T), where: $t_0 < t_1 < \ldots < t_K < t_0+T$. Consider the problem of estimating the initial phase parameter θ_0 based on the observed realization of the Poisson process, $\{t_k\}$. The rate function of the Poisson process has the functional form,

$$\Lambda(t;\theta_0) = \beta + \alpha\, h[\theta_0 + \theta(t)] \tag{12}$$

where the effective source and background photon rates, α and β, are known. Additionally, the normalized pulse profile $h(\phi)$, the observed signal frequency $f(t)$, and hence the accumulated phase function $\theta(t)$, are also assumed known. The log-likelihood for this problem is given by the expression [19],

$$L\left(\{t_k\};x\right) = \sum_{k=1}^{K} \log\left[\Lambda(t_k;x)\right] + \int_{t_0}^{t_0+T} \Lambda(t;x)\;dt \tag{13}$$

where log denotes the natural logarithm, and x is the value of θ_0 at which the log-likelihood function is evaluated. The dependence of the second term on x becomes negligible as T spans many periods of $\Lambda(t)$, or rather if $\theta(t_0+T) \gg 1$. The maximum-likelihood (ML) estimate of the desired parameter is obtained by solving the optimization problem,

$$\hat{\theta}_0 = \underset{x\in(0,1)}{\arg\max}\; L\left(\{t_k\};x\right) \tag{14}$$

which can be solved numerically using an iterative grid-search algorithm. If the observed signal frequency is constant over the observation interval, or $f(t) = f$ for $t \in (t_0, t_0 + T)$, then the ML phase estimate takes on the special form (ignoring the integral term of the log-likelihood expression):

$$\hat{\theta}_0 = \arg\max_{x \in (0,1)} \sum_{k=1}^{K} \log\left[\beta + \alpha\, h\left(\, x + f[t_k - t_0]\right)\right] \tag{15}$$

The phase estimation problem described assumes that frequency of the observed signal, whether fixed or time varying, is known ideally over the observation interval. This includes knowledge of any Doppler shifts that may cause the observed signal frequency to vary as the spacecraft moves towards or away from the X-ray source over the observation interval. If the frequency shifts due to Doppler (or the spacecraft velocity projected in the source line-of-sight direction) is not known to sufficient accuracy, then formulation of a two-dimensional ML search algorithm is possible for joint estimation of the phase and frequency parameters. This problem, however, is not addressed in the current paper and will be investigated in future work. In the following, the observed frequency of each X-ray source is assumed to be known ideally.

Cramer-Rao Performance Bound

When pulses arrive periodically (every P seconds), a one-to-one relationship is established between the phase parameter θ_0 and pulse time-of-arrival (TOA), since $\theta(t)$ becomes:

$$\theta(t) = \frac{t - t_0}{P}, \quad \text{and} \quad \Lambda(t;\theta_0) = \Lambda(t + \tau; 0) \tag{16}$$

where $\tau = P\theta_0$ is a time shift parameter. In other words, the problems of phase estimation (modulo one cycle) and pulse TOA estimation (modulo P seconds) become essentially the same. As a result, not only are the phase estimation error, $\delta\theta_0$, and the pulse TOA estimation error, $\delta\tau$, related to each other, but they are also related to the range estimation error, $\delta\rho$, according to the equation: $\delta\rho = c(\delta\tau) = cP(\delta\theta_0)$.

The ML estimation of pulse TOA has been thoroughly analyzed in [19]. An approximate mean-square error expression was derived {see Eq. (42) of [19]}, which is specialized below for the case of a periodic rate function with $T \gg P$ and stated in terms of the root-mean-square (RMS):

$$\sigma_{TOA} \equiv \sqrt{E(\delta\tau^2)} \geq \left\{ \frac{T}{P} \int_0^P \frac{\left[\alpha \dfrac{d}{dt} h\left(t/P\right)\right]^2}{\alpha\, h\left(t/P\right) + \beta}\, dt \right\}^{-\frac{1}{2}} = \left\{ \frac{T}{P^2} \int_0^1 \frac{\left[\alpha \dfrac{d}{d\phi} h\left(\phi\right)\right]^2}{\alpha\, h\left(\phi\right) + \beta}\, d\phi \right\}^{-\frac{1}{2}} \tag{17}$$

The inequality $\geq$ is used in the above formula because evaluation of the Cramer-Rao bound (CRB) produced the same expression, and the CRB is a lower-bounding expression that pertains to all unbiased estimators [20]. The CRB on range estimation error can be obtained by simply multiplying the pulse TOA accuracy by the speed of light: $\sigma_{RANGE} = c\,\sigma_{TOA}$. Note that evaluation of the CRB requires only knowledge of α, β, $h(\phi)$, P, and T.

Numerical Results

Performance of the ML estimator was evaluated using the Monte-Carlo technique. Photon arrival times were generated as a realization of the Poisson point process over the observation interval and then subsequently processed by the ML algorithm to solve for the phase parameter estimate. This process was repeated for many realizations of the Poisson process (400 Monte-Carlo runs), and the RMS phase error was calculated through empirical averaging of the squared phase estimation error. The numerical results are reported as range accuracies: $\sigma_{RANGE} = cP\,\sigma_{PHASE}$ in Table 2 for a selection of pulsars. The Cramer-Rao bound was also calculated for the same set of pulsars, and the results of these calculations are also shown in Table 2 for a side-by-side comparison against the ML simulated performance. Where the ML estimator performs at or near the CRB, it is performing as an optimal or near-optimal estimator. This is an indication that the pulsar is observed sufficiently long to guarantee that the ML estimator is not operating in a photon-limited region of operation [19]. The CRB lower bound and ML estimator performance for two pulsars are plotted as function of observation time in Figure 2. Photon-limited performance regions are apparent in the results where the CRB and ML performances do not coincide; however beyond an observation time threshold, the ML estimator achieves the CRB performance and improves linearly with observation time.

Table 2
X-RAY SOURCES CHARACTERISTICS AND RANGE MEASUREMENT ACCURACY

Pulsar Name	Period (s)	X-ray Flux (ph/cm^2/s) (2-10 keV)	Pulsed Fraction (%)	σ_{RANGE} (km)		Reference
				CRB (after 500 s)	ML (after 500 s)	
PSR B1937+21	0.00156	4.99E-05	86	2.27	2.28	[21, 22]
PSR J0218+4232	0.00232	6.65E-05	73	3.95	7.00	[21, 23]
PSR B0540-69	0.0504	5.15E-03	67	22.4	23.0	[21, 23]
PSR B1509-58	0.150	1.62E-02	65	32.6	32.6	[21, 23]
SAX J1808.4-3658	0.00249	3.29E-01	7	1.20	1.20	[24, 25]
PSR B1821–24	0.00305	1.93E-04	98	2.34	2.60	[21-23]
XTE J1814-338	0.00318	3.88E-02	12	3.68	3.68	[26]
PSR B0531+21	0.0334	1.54E+00	70	0.168	0.168	[21, 23]

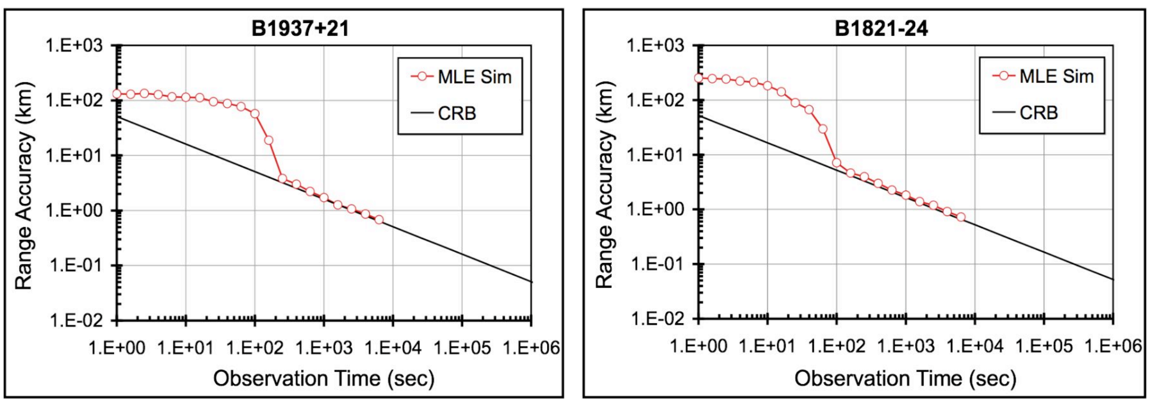

Figure 2. CRB and ML simulation plots for two pulsars.

MEASUREMENT DIFFERENCES

In order to compute the absolute position of a detector using variable celestial sources, it is necessary to determine which specific pulse is arriving at the detector from a source. Since sources do not specifically identify any of the pulses that they emit, each pulse must be identified through joint observations of pulses from multiple pulsars. Figure 3 shows the arrival of pulses at a spacecraft from several pulsars. At any given instance, there is only one unique set of pulse phases from this group of pulsars that solves for the exact location of the vehicle. Due to the significant distances between these celestial sources and the solar system, the pulse waves that arrive into the system are assumed to be planar, not spherical. Ignoring the spherical effects of the wave propagation is only significant if the spacecraft and location of the model used for comparison are very far apart.

Since no identifying information is provided with each pulse from a pulsar, directly determining which specific pulse is arriving at a given instance is not possible. However, by defining a pulse-timing model at a known location, it is possible to identify the set of *differences* in pulses between the spacecraft and the known location. The pulse-timing model is defined at a specific location within an inertial frame. Any specified location can be used, however, the most common location is the solar system barycenter (SSB) origin [14, 15]. For a single pulsar, a measured difference can be created with the pulse arrival time at the detector and the predicted arrival time at the known location. The difference in these values immediately identifies a set of candidate positions along the line-of-sight to the pulsar. These candidate locations are the value of measured fraction of pulse phase plus or minus multiple whole value pulse cycle lengths. Only one unique position satisfies the measured differences from a set of pulsars; and once this unique position is identified, the correct set of differenced cycles are immediately determined. The methods of determining absolute position rely on the difference of phase between the spacecraft and the model's defined location. If this location is far from the spacecraft, then many pulse cycles will exist between the two locations. If this location is relatively close to the spacecraft, then it is possible that only a fraction of a pulse cycle exists between the two locations.

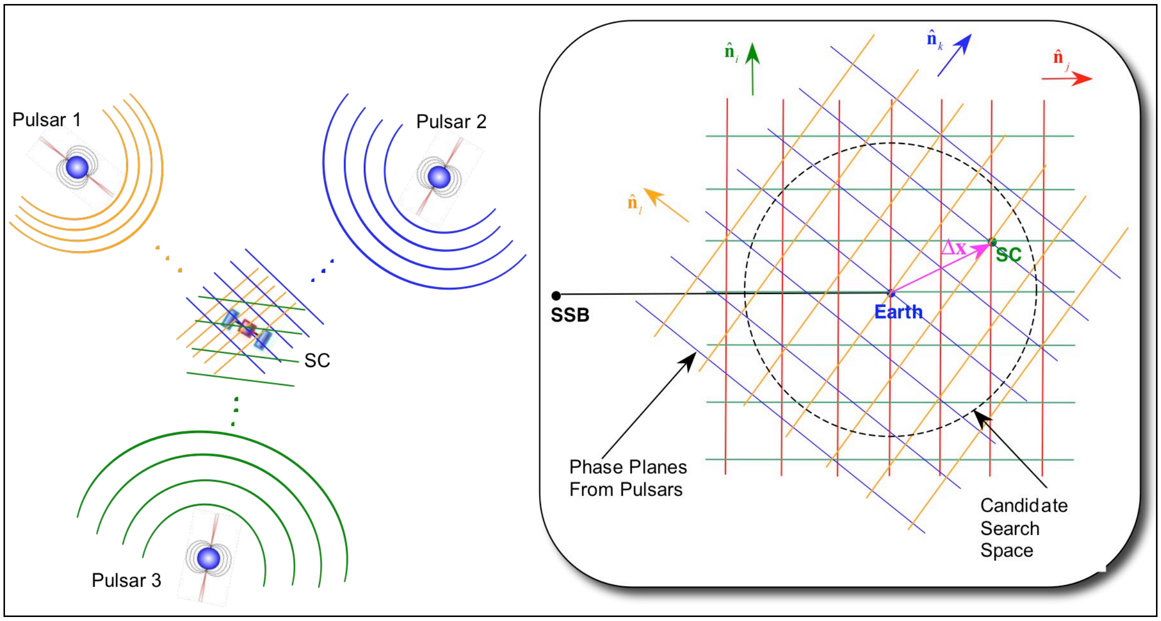

Figure 3. Pulse arrivals from individual pulsars at spacecraft location.

For spacecraft orbiting Earth, one method to avoid accumulating pulse cycles between the vehicle's detector and the SSB is to use pulsars with large periods. Using sources with periods greater than 500 sec $\left(>1\,AU/c\right)$ ensures there is only one cycle between the SSB and Earth. Long period pulses, however, also require longer observation time, which may be detrimental to spacecraft operations if a fast absolute position solution is required. An improved method for ensuring that only a few cycles exist between the spacecraft and the pulse model location is to keep the model's defined location *close* to the spacecraft. For spacecraft orbiting near Earth a better pulse model location would be at the geocenter (Earth-center), or perhaps the Earth-Moon barycenter. Although these locations are not truly inertial locations, compensations in the pulse models as well as short observation times would allow these locations to be used. Alternatively, any location near the spacecraft could be used for the model location. For example, a spacecraft orbiting Mars or Jupiter could use the center of those planets or their system's barycenter. These methods require redefining existing pulsar timing models defined at the SSB at these new locations.

Several types of measurement differences are described below. The *Single Difference* is the difference between the measured phase at the detector and the phase predicted at a model location for a single pulsar. The *Double Difference* is the subtraction of two single differences from two separate pulsars. The *Triple Difference* is the subtraction of two double differences between two separate time epochs. The benefits of computing these differences include removing immeasurable errors, with higher order differences removing additional errors. The complexity of using higher order differences includes requiring more observable sources to produce solutions, which may take additional observation time. The errors within these difference equations that are expected to be present in an actual navigation system can also be calculated, and the interested reader is referred to [9].

Single Difference

Measurements of the pulsed radiation from variable celestial sources can be differenced from the predicted arrival time from a pulse-timing model. For the examples shown below, the location of Earth within the SSB inertial frame will be used for illustrative purposes. The single difference removes any values common to both the spacecraft and the model location. Primarily, it removes the pulsar distance, which is often not known to sufficient accuracy. Measurement differences can be created using measured range from the source or measured cycle phase. Primarily the phase measurements will be used in these algorithms to compute spacecraft position; however, the range measurement algorithms are provided to help illustrate the methods described here.

Range Single Difference

The vectors between the pulsar source and Earth and between the pulsar and the spacecraft are shown in Figure 4. The source is assumed to be extremely far away from the solar system, and the difference in these range vectors provides an estimate of the offset between Earth and the spacecraft, $\Delta\mathbf{x}$.

Considering only the geometric representation from Figure 4, the position of the spacecraft relative to Earth can be represented using the spacecraft's position, $\mathbf{r}_{SC}$, and Earth's position, $\mathbf{r}_E$, within the SSB inertial frame as,

$$\Delta\mathbf{x} = \Delta\mathbf{r} = \mathbf{r}_{SC/E} = \mathbf{r}_{SC} - \mathbf{r}_E \tag{18}$$

Since the pulsar is so distant, the line-of-sight can be considered constant, or $\hat{\mathbf{n}} \approx \hat{\mathbf{n}}_{SC} \approx \hat{\mathbf{n}}_E$. Therefore, the difference in magnitude of range represents the spacecraft's position along the line-of-sight to the pulsar as,

$$\Delta\rho_i = \rho_{E_i} - \rho_{SC_i} = \hat{\mathbf{n}}_i \cdot \Delta\mathbf{x} \tag{19}$$

Including the relativistic effects on the light ray path from the pulsar to either the spacecraft or Earth from Eq. (4), a simplified form of the range difference becomes,

$$\Delta\rho_i \approx \hat{\mathbf{n}}_i \cdot \Delta\mathbf{x} + \left[RelEff_{E_i} - RelEff_{SC_i} \right] \tag{20}$$

Eq. (20) shows that implementing a single difference removes the poorly known pulsar position vector, $\mathbf{D}$, from Eq. (4). Thus, this form of spacecraft position computations does not rely on a range measurement directly from the pulsar.

Phase Single Difference

The single-phase difference represents the fraction of cycle phase, or fraction of phase plus a fixed number of integer cycles, from an arriving pulse between the spacecraft and the model location. The insert of Figure 4 provides a diagram of arriving pulses from a single celestial source at a spacecraft and Earth. Using multiple measured phase differences from different sources provides a method of determining the spacecraft's three-dimensional position with respect to Earth in an inertial frame. Phase difference is directly related to range difference when the wavelength, λ, of the cycle is included. The geometric relationship of the single-phase difference can be expressed as,

$$\lambda_i \Delta\Phi_i = \lambda_i \left(\Delta\phi_i + \Delta N_i \right) = \lambda_i \left[\left(\phi_{E_i} - \phi_{SC_i} \right) + \left(N_{E_i} - N_{SC_i} \right) \right] = \Delta\rho_i = \hat{\mathbf{n}}_i \cdot \Delta\mathbf{x} \tag{21}$$

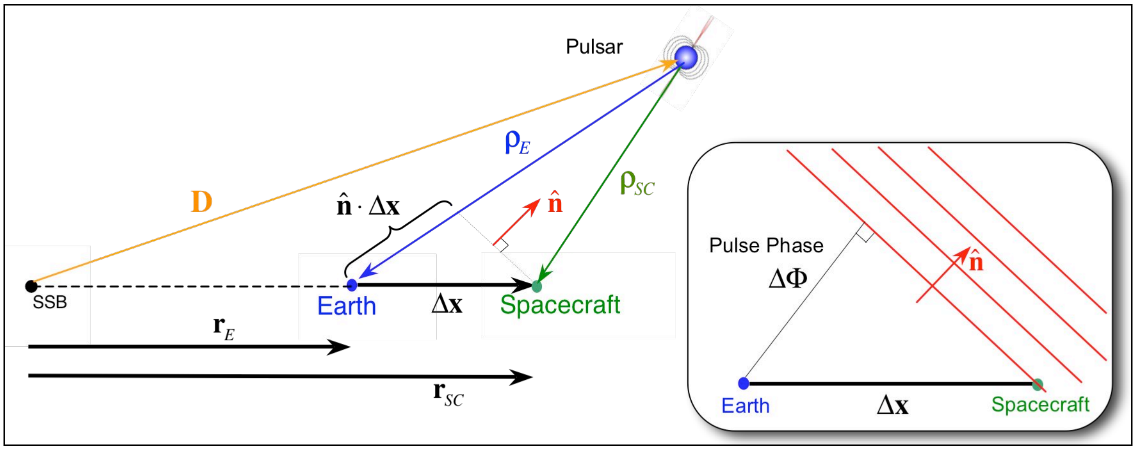

Figure 4. Range vectors from single pulsar to Earth and spacecraft locations, including pulse phase.

Double Difference

A double difference is the subtraction of two single differences from two separate pulsars. This difference removes values that are common to both pulsars, such as navigation system dependent values. However, double differences require observations from multiple sources to be conducted contemporaneously, such that the pulse arrival time measurements from these sources are computed simultaneously and at the same position of the spacecraft. This may require multiple detectors to be integrated into a single system for full absolute position determination. Otherwise, methods must be employed to adjust arrival times for observations made at different times to the same time epoch.

Range Double Difference

The range double difference is computed between these two sources, the i^{th} and j^{th} pulsars. The diagram in Figure 5 shows the arriving pulses from two pulsars into the solar system. Including the effects of relativity on the light ray path for range single differences as in Eq. (20), the range double difference for two pulsars becomes the following equation. In this expression, the symbol ∇ is used to represent a double difference, and should <u>not</u> be misinterpreted as the *gradient* operator.

$$\nabla\Delta\rho_{ij} \cong \left(\rho_{E_i} - \rho_{SC_i}\right) - \left(\rho_{E_j} - \rho_{SC_j}\right) \cong \left(\hat{\mathbf{n}}_i - \hat{\mathbf{n}}_j\right) \cdot \Delta\mathbf{x} + \left[\Delta RelEff_i - \Delta RelEff_j\right] \tag{22}$$

Phase Double Difference

Figure 5 provides a diagram of the phase single difference for two pulsars, which can be subtracted from one another to produce a phase double difference. The total phase double difference is composed of the fractional phase double difference and the integer cycle double difference, and is given by,

$$\nabla\Delta\Phi_{ij} = \nabla\Delta\phi_{ij} + \nabla\Delta N_{ij} \cong \left(\frac{\hat{\mathbf{n}}_i}{\lambda_i} - \frac{\hat{\mathbf{n}}_j}{\lambda_j}\right) \cdot \Delta\mathbf{x} + \left[\frac{\Delta RelEff_i}{\lambda_i} - \frac{\Delta RelEff_j}{\lambda_j}\right] \tag{23}$$

Triple Difference

The triple difference is created by subtracting two double differences at two separate time epochs. This difference removes any values that are not time dependent. For a static system or when measurements are made over fairly short difference in time, many of the time independent terms will cancel.

Range Triple Difference

The triple difference for range can be computed from Eq. (22) at times t_1 and t_2 as,

$$\nabla\Delta\rho_{ij}(t_2) - \nabla\Delta\rho_{ij}(t_1) \cong \{\hat{\mathbf{n}}_i - \hat{\mathbf{n}}_j\} \cdot [\Delta\mathbf{x}(t_2) - \Delta\mathbf{x}(t_1)] + \begin{bmatrix} \nabla\Delta RelEff_{ij}(t_2) \\ -\nabla\Delta RelEff_{ij}(t_1) \end{bmatrix} \tag{24}$$

For most applications, the triple difference of the relativistic effect can be considered to be very small, so thus the range triple difference can be stated as,

$$\nabla\Delta\rho_{ij}(t_2) - \nabla\Delta\rho_{ij}(t_1) \cong \{\hat{\mathbf{n}}_i - \hat{\mathbf{n}}_j\} \cdot [\Delta\mathbf{x}(t_2) - \Delta\mathbf{x}(t_1)] \tag{25}$$

Phase Triple Difference

The phase triple difference can be computed using Eq. (23). If all the triple differences with respect to relativity effects are considered negligible, then the phase triple difference can be written as,

$$\begin{aligned} \nabla\Delta\Phi_{ij}(t_2) - \nabla\Delta\Phi_{ij}(t_1) &= [\nabla\Delta\phi_{ij}(t_2) - \nabla\Delta\phi_{ij}(t_1)] + [\nabla\Delta N_{ij}(t_2) - \nabla\Delta N_{ij}(t_1)] \\ &\approx \left\{\frac{\hat{\mathbf{n}}_i}{\lambda_i} - \frac{\hat{\mathbf{n}}_j}{\lambda_j}\right\} \cdot [\Delta\mathbf{x}(t_2) - \Delta\mathbf{x}(t_1)] \end{aligned} \tag{26}$$

If the time difference is short enough, and the phase cycle is long enough, then the integer cycle will not change between measurements and the integer cycle triple difference from Eq. (26) will be zero, or $[\nabla\Delta N_{ij}(t_2) - \nabla\Delta N_{ij}(t_1)] = 0$. This simplifies the expression, and provides an expression for spacecraft position using only the fractional phase measurements.

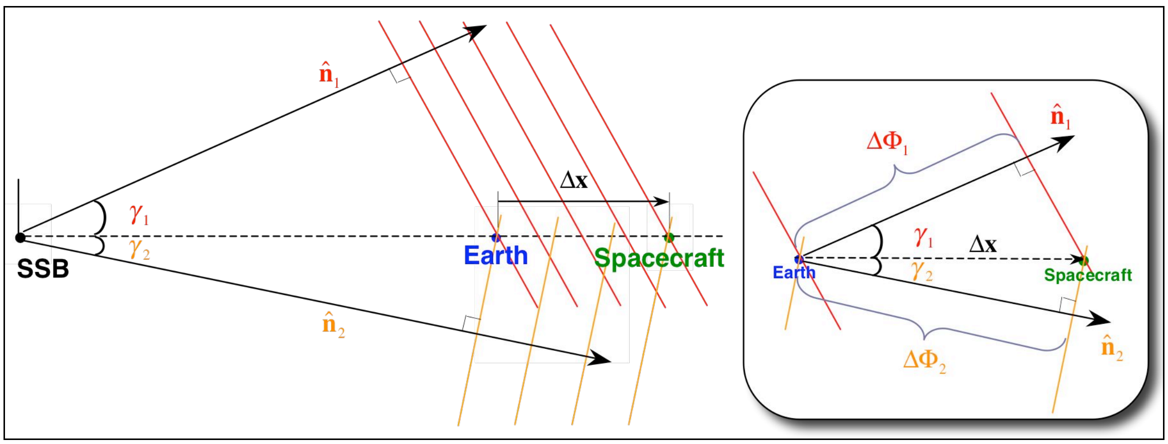

Figure 5. Pulse plane arrivals at the spacecraft and Earth from two separate sources.

SEARCH SPACE AND CYCLE AMBIGUITY RESOLUTION

The *pulse phase cycle ambiguity resolution* processes rely on the fact that for a given fully determined set of phase measurements from separate pulsars, there is one unique position in three-dimensional space that satisfies all the measurements. Thus, there is only one fully unique set of cycles that satisfies the phase measurements. Once this set of cycles is identified, the three-dimensional position can be determined by adding the fractional portion and integer number of phase cycles that are present between the spacecraft and the reference location.

The solution cycle set may be selected using a *search space*, or three-dimensional geometry that contains an array of candidate cycle sets. Each set within a chosen search space is processed and the likelihood of each set being the unique solution is tested. Individual candidates that satisfy processing tests are retained for further evaluation. Using sufficient measurements from enough pulsars allows a unique cycle set within the search space to be chosen as the most likely set for the position of the spacecraft. Testing each candidate set of cycles within a large search space can be computationally intensive and may require large processing time. Methods that help reduce the search space, or more quickly remove unlikely candidates, are a benefit to the computations. Additionally, multiple tests of the candidate sets, which help identify likely candidates, improve the efficiency of the selection process.

In an actual navigation system, errors that are present within the system will cause the candidate selection process to be less accurate. Within the direct solution methods, errors may cause incorrect cycle sets to be identified. Within the search space methods, errors cause multiple candidate sets to be retained until the correct solution can be identified. Thus, all attempts must be made to insure that *i*) selection methods guarantee that the correct solution is a potential solution, *ii*) the true candidate set lies within the chosen search space, *iii*) test criteria must account for measurement noise within the system, and *iv*) any chosen set of cycles must be continually monitored to insure its validity.

Search Space

Creating a sufficient search space is critical for accurate cycle identification and position determination. The candidate cycle sets within a search space are defined by the single, double, or triple differences. The search space is typically symmetrical about its origin. The origin, or center point, of the search space would often be chosen as the pulsar timing model location, in accordance to where the single-, double-, and triple-differences are to be computed. Candidate cycles can exist within the search space on either side of the origin, unless some prior knowledge allows the removal of candidates from one side of the origin. To solve for a vehicle's *lost-in-space* problem, a better choice for the search space origin is the vehicle's last known position, if this is continually stored in backup memory onboard the vehicle. Once a search space has been generated, it is possible to reduce the number of sets to be searched by removing those sets that are known to exist inside any planetary bodies, as spacecraft could not physically be located inside these bodies.

The insert of Figure 3 shows a diagram of a candidate cycle search space in two dimensions. The SSB, Earth, and spacecraft positions are shown, and arriving pulse phase planes are diagramed arriving from four different pulsars. The spherical geometry search space is shown as centered about Earth. The only candidate set of cycles within the search space that has all phase planes crossing in one location is the true location of the spacecraft. Three methods can be considered in creating a cycle search space. The *Geometrical Space* creates a cycle search space by placing a three dimensional geometrical boundary about the origin, such as a sphere or cube of specified dimensions, or an ellipsoid, perhaps about the planet's equatorial plane. The dimensions of this geometry, centered about the origin, define the candidate cycles along the line-of-sight vector to each pulsar. The search space candidate sets are selected such that they lie within this geometrical boundary. A *Phase Cycle Space* can be defined as a fixed number of cycles along the line-of-sight to a pulsar. The number of cycles considered can be specific to each pulsar. For example, a choice of ten cycles on each side of the origin could be selected for a pulsar. If the pulse cycle length from each pulsar is sufficiently different, care must be taken in order to ensure that the true cycle set is maintained within the created search space. A *Covariance Space* is defined by the covariance matrix of the measurements given a set of pulsar phase observations and their measurement noise. The covariance matrix will skew the search space based on the magnitudes of the uncertainties. The search space shape is ellipsoidal oriented along the eigenvectors of the covariance matrix [27].

Cycle Ambiguity Resolution

Once a search space has been defined, three phase cycle ambiguity resolution methods could be pursued [9, 11]. Each method has advantages for specific applications, and some require less processing than the others. The *Batch*, or *Least Squares*, method directly solves for cycle ambiguities based upon input measurements. Processing is fairly simple, but requires intelligent pre-processing, and inaccurate measurements can lead to widely erroneous results. The *Floating-Point Kalman Filter* method generates a floating-point estimate of the integer cycle ambiguity set as produced by the observing Kalman filter.

Somewhat process intensive, this method may require large amounts of measurement data over time in order to resolve the correct ambiguity set. The *Search Space Array* method exhaustively tests each potential cycle set that exists within a created search space. Although process intensive if large amount of candidate sets exist within a search space, with the use of well-chosen selection tests this method can typically correctly resolve the cycle ambiguities. This paper will concentrate on the *Search Space Array* technique.

Once a position solution is computed, providing an estimate of its accuracy is important for many operations. The *Floating-Point Kalman Filter* and *Search Space Array* methods provide accuracy estimates as part of their processing. Utilizing the Geometric Dilution of Precision (GDOP) is also a beneficial performance quantity [9, 10]. These concepts allow an assessment of the quality of the computations.

Search Space Array Resolution

Use of this resolution technique assures that the correct solution set will be tested, rather than potentially never being evaluated by other methods. Intelligent search space creation helps reduce the exhaustive processing by limiting the number of candidate sets. In order to evaluate each candidate cycle set, a comprehensive test of the candidate's validity and accuracy must be performed. From Eq. (21), for a phase single difference from one pulsar, using the measured phase difference, $\Delta\phi$, and a chosen set of cycle differences, $\Delta\tilde{N}$, the spacecraft position along the line-of-sight for the pulsar can be solved for using,

$$\hat{\mathbf{n}}_i \cdot \Delta\tilde{\mathbf{x}} = \lambda_i \left(\Delta\phi_i + \Delta\tilde{N}_i\right) \tag{27}$$

Given a set of at least three pulsars, the measurements can be assembled as,

$$\begin{bmatrix} \hat{\mathbf{n}}_1 \\ \hat{\mathbf{n}}_2 \\ \hat{\mathbf{n}}_3 \end{bmatrix} \Delta\tilde{\mathbf{x}} = \mathbf{H}\Delta\tilde{\mathbf{x}} = \begin{bmatrix} \lambda_1\left(\Delta\phi_1 + \Delta\tilde{N}_1\right) \\ \lambda_2\left(\Delta\phi_2 + \Delta\tilde{N}_2\right) \\ \lambda_3\left(\Delta\phi_3 + \Delta\tilde{N}_3\right) \end{bmatrix} \tag{28}$$

The spacecraft position can then be solved for using a matrix pseudo-inverse,

$$\Delta\tilde{\mathbf{x}} = \left[\left(\mathbf{H}^T\mathbf{H}\right)^{-1}\mathbf{H}^T\right] \begin{bmatrix} \lambda_1\left(\Delta\phi_1 + \Delta\tilde{N}_1\right) \\ \lambda_2\left(\Delta\phi_2 + \Delta\tilde{N}_2\right) \\ \lambda_3\left(\Delta\phi_3 + \Delta\tilde{N}_3\right) \end{bmatrix} \tag{29}$$

Using this value for spacecraft position, any additional pulsars $\left(j > 3\right)$ can have their cycle ambiguities directly solved for using an integer rounding function as,

$$\Delta\tilde{N}_j = round\left(\frac{\hat{\mathbf{n}}_j}{\lambda_j} \cdot \Delta\tilde{\mathbf{x}} - \Delta\phi_j\right) \tag{30}$$

A *residual test* can be generated using these new estimated cycle ambiguities as,

$$\nu_j = \frac{\hat{\mathbf{n}}_j}{\lambda_j} \cdot \Delta\tilde{\mathbf{x}} - \Delta\phi_j - \Delta\tilde{\mathbf{N}}_j \tag{31}$$

If more than one additional observed pulsar is available, then a vector of these residual tests can be assembled as $\boldsymbol{\nu} = \left[\nu_j \quad \nu_{j+1} \quad \cdots \quad \nu_k\right]^T$. The magnitude of this residual vector provides an estimate of the quality of the computed spacecraft position, $\Delta\tilde{\mathbf{x}}$,

$$\sigma_\nu = norm\left(\boldsymbol{\nu}\right) \tag{32}$$

Each candidate set within a search space can be evaluated using this test statistic, σ_ν. If the chosen set does match well, then the differences for each extra observable pulsar from Eq. (31) will be small and consequently, the magnitude of the residual vector will be small. Likewise, if a chosen set does not match well with the measured phase difference and spacecraft position, then the value of residual will be large. A threshold for this residual magnitude can be chosen in order to remove many, if not all, of the candidate sets other than the specific candidate set that represents the true spacecraft position. If several candidate sets remain below a chosen threshold, additional measurements from pulsars can help to eliminate wrong candidate sets. Eventually, after enough measurements have been processed, the true candidate set will be identified and the absolute position of the spacecraft will be determined.

The residual vector within Eq. (32) can be defined using double and/or triple phase and cycle differences. However, because these higher order differences are evaluated using differences of close or similar values developing a test statistic threshold that sufficiently removes unwanted candidate sets and retains the correct candidate set becomes increasingly difficult. In order to augment this issue, *combined-order* systems, where candidate set evaluation is performed at multiple levels of differences can assist in selecting the correct cycle set. For example a combined-order system incorporating both first and second differences may help to identify the correct cycle set.

RELATIVE POSITION

The preceding sections developed methods to determine a spacecraft's absolute position within an inertial frame. Some applications, however, may only require knowledge of *relative position*, or the position relative to a location that may or may not be fixed. This relative, or *base station*, location may be the position of another vehicle or any object that the spacecraft uses as a relative reference. Since this base station's relative location may not be known by the spacecraft at any given instance, the location of this relative object must be transmitted to the spacecraft when measurements are needed. The diagram of Figure 6 provides the relative navigation concept with a base station spacecraft and a single remote spacecraft. Communication between the remote spacecraft and the base station, as well as contemporaneously measured pulse arrival times, allows relative navigation of the vehicles. If the base station also has a detector, similar to the spacecraft, then direct phase measurement difference comparisons can be implemented instead of using a pulse-timing model. If a pulse-timing model is used, the base station must transmit its location so that the inertial-based timing model can be transferred to the base station's location.

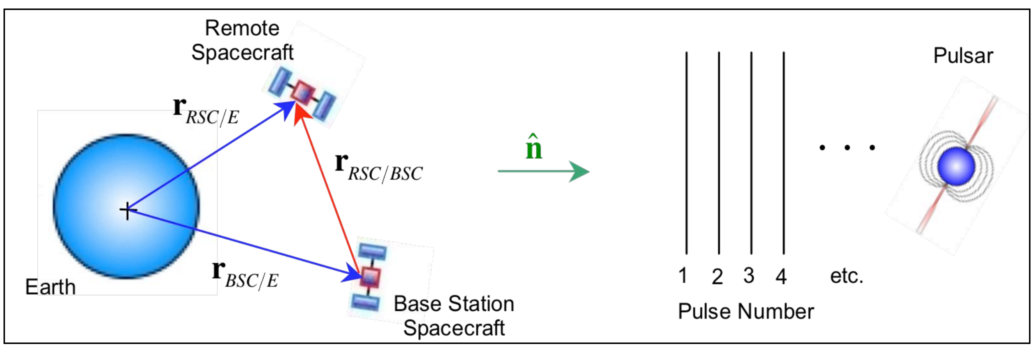

Figure 6. Position of remote spacecraft relative to base station spacecraft.

This relative navigation system requires more processing due to the extra communication and because the system is a dynamically operating system versus a static base station. Time alignment of measurement date is crucial and often complicated. This type of navigation has similarities to the processes of differential or relative GPS navigation, where one receiver station transmits its information to another station in order to determine relative position and velocity information [3]. For spacecraft operating in near-vicinity to one another, linear approximations to their relative equations of motions can provide additional simplifications to this relative navigation process. The Clohessy-Wiltshire-Hill equations describe this type of motion between two orbiting vehicles when they are relatively close and they have similar orbit parameters [28].

Relative navigation is useful for applications such as multiple spacecraft formation flying, a spacecraft docking with another vehicle, or a rover operating on a planetary body with respect to its lander's base station. Alternatively, a base station satellite can be placed in Earth orbit and be used to monitor and update pulsar ephemeris information. Ideal locations for these base stations may include geosynchronous orbits (GEO), Sun-Earth and Earth-Moon Lagrange points, or solar-system halo orbits. Once new or updated pulsar data is computed, the base station could broadcast this information to all operational spacecraft. This method may provide improved accuracy over the absolute position method, since the base station can provide real-time updates of pulse models.

NUMERICAL SIMULATION

In order to test the methods presented above for position determination of a spacecraft, a simulation of the algorithms has been developed. Below is a description of the implementation of the simulation, as well as some representative performance results.

Simulation Description

The intent of the simulation is to determine the unknown integer pulse cycles of the total phase difference from each source between a known reference location and the true location of the spacecraft. A search space is created to identify candidate sets of integer cycles that would produce the most likely position of the spacecraft based upon the measured fractional pulse phase differences between the reference location and the spacecraft. The simulation has been primarily developed to investigate the position of vehicles near-Earth, and the geocenter was chosen as the reference location. The simulation is also designed to perform studies of relative position determination between two vehicles.

The simulation creates a geometrical search space using a reasonable distance from Earth for a specific spacecraft. The search space is in the form of a spherical shell and is centered about the geocenter. The bounds of the shells are defined by a minimum radius, such as the radius of Earth, and a maximum radius, such as several times the expected orbit radius of the vehicle. Only sets of candidate integer cycles that compute position within these bounds are considered acceptable and processed within the simulation.

The set of eight variable X-ray sources was selected from Table 2 for use within the simulation. It was assumed that each source could be observed simultaneously for duration of 500 seconds, which would require multiple detectors acting in unison to produce pulse phase measurements from each source at the same instance, or would require additional methods to time align all the phase measurements. To begin the processing, each source's pulse arrival time was computed assuming the detector was located at the geocenter. However, a vehicle's detector will measure a pulse TOA that is offset from the predicted TOA of a pulse-timing model at the geocenter due to the vehicle's true position offset from the geocenter. The true phase difference is in terms of both fractional phase cycle and an integer number of cycles. The algorithms within the simulation determine the unknown integer number of cycles based upon the fractional phase difference measurements.

There are two main processing loops within the simulation that implements a combined order system, using both a phase double difference loop and a phase single difference loop. Within the double difference loop, the first four sources from Table 2 (the shaded rows) are used along with each combination of their integer cycle candidates within the defined search space to compute a position offset from the geocenter as in Eq. (23). The sources were selected based upon their cycle wavelengths and their good GDOPs. The computed position from this set of four sources is verified to exist within the search space. This estimated position is then used to compute a residual as in Eq. (32) for each of the four remaining sources from the table. The magnitude of this residual is compared to a test statistic threshold value. The full set of candidate cycles that pass the residual threshold test are recorded and passed to the single difference loop.

The second loop within the simulation computes a position based upon the phase measurements and all the search space candidates that passed the double difference residual test. This new position is first verified to exist within the defined search space. Those positions that pass the search space geometry test are then used along with their phase measurements and candidate cycles to compute a single difference residual vector for all eight sources. Those candidate sets that pass a single difference threshold residual test are recorded. For many runs of the simulation, the set of cycles that computes the smallest single difference residual is the set that computes the correct spacecraft position.

To simulate errors within the phase measurements, several effects have been included. The range accuracy – converted to phase using the cycle wavelength – from Table 2 simulates the expected phase measurement performance from each source. A 2% additional phase error was included, which represents variations due to source intensity fluctuations, X-ray background noise, and instrument errors. These terms are root-sum-squared and multiplied by a normalized random number, in order to represent a random component of the full error. This error was then added to a phase bias error to produce the total phase error. The phase bias error was produced to represent the uncertainty of vehicle velocity affecting the pulse TOA computations, and was chosen at 5% of true velocity. Additional studies were pursued to investigate the consequences of utilizing fewer pulsars for an observation. Therefore, the simulation was also executed with the transient sources SAX J1808.4-3658 and XTE J1814-338 removed from the pulsar list. These sources were specifically chosen due to their transient nature to show benefits of considering all types of sources. However, being able to operate with fewer sources can benefit many applications.

For some simulation runs, there are several single differenced candidate sets that compute residuals that are smaller than the candidate set of the true solution. For these candidate sets, even though they compute small residuals, their position solutions are often grossly incorrect. This is due to the contributions of phase error affecting the residual computations. In these circumstances, further tests must be pursued to determine which of the multiple potential solutions is correct. This may include processing another complete observation set, which would expose those incorrect solution sets and help identify the correct solution from both observations.

Simulation Results

Several test cases have been investigated using this simulation. Presented below are simulations of the position determination of spacecraft within the GPS and GEO orbits. Each case has a specifically defined search space. The dimensions of each search space are provided in Table 3. For the GPS orbit, spherical shells are created about the geocenter, since these spacecraft could be anywhere within this three-dimensional region. The DirecTV 2 spacecraft was chosen to represent satellites in GEO, where the spherical shell search spaces are truncated along the z-axis, since these vehicles would orbit close to the equator. This table also presents the selected threshold values for the double difference and single difference residual tests used in the simulation. Orbit data of each spacecraft's orbit was provided by the NORAD Two-Line Element (TLE) sets [29, 30]. The chosen epoch that defines the position of the vehicle within its orbit is provided in Table 3.

Table 4 presents example simulation results for determining the correct set of cycle candidates within the GPS and DirecTV 2 spacecraft orbits. Using the first four pulsars from Table 2, within the known GPS orbit radius of 26575 km, there are initially 138,645 candidates cycle sets that are investigated. Of these candidates, only 32,803 sets remain within the defined search space shell of Table 3. Using the threshold value from Table 3, 27,789 candidates remain after the double difference residual tests using the remaining four pulsars. Then incorporating all eight sources to define the single difference position solution for each set, 25,569 candidates remain within the search space region. Finally, after computing the single differenced residual test, using the first source of Table 2 as the primary source, only three candidate sets are found to pass the test. Of these three candidates, the set with the smallest value from the single difference residual test is the correct solution. This demonstrates that exhaustively testing each possible candidate set can correctly identify the true vehicle position. When using only six pulsars, a similar reduction in candidate sets is evident. However, three potential candidate sets have a single difference residual that is smaller than the true position solution set. Of each of these remaining sets only one computes a position that is within 2000 km of the GPS orbit radius. All four sets would need to be re-evaluated with respect to the GPS orbit or continually monitored to determine which is the correct solution.

In the DirecTV 2 orbit, since the search space region is much larger than in the GPS orbit case, there are many more initial candidate sets that must be investigated. However, this large number of candidates is quickly reduced when tested to exist within the search space region and tested against the double difference residual threshold. For this specific run, with eight pulsars being observed the correct solution is identified with the smallest single difference residual. For the case of six pulsars, only one candidate other than the true solution has residuals less than the true set, but is located over 9,000 km from the GEO orbit radius.

Table 3
SIMULATED ORBIT SEARCH SPACE AND THRESHOLD DATA

Spacecraft Orbit	Epoch (JD)	Search Space (km)	Double Difference Residual Threshold	Single Difference Residual Threshold
GPS BIIA-16 PRN-01	2453345.820344930	R_{min} = 20025 R_{max} = 33375	8 Pulsars: 0.70 6 Pulsars: 0.40	8 Pulsars: 0.07 6 Pulsars: 0.04
DirecTV 2 (DBS 2)	2453372.624232230	R_{min} = 31500 R_{max} = 52500 z_{max} = ±10000	8 Pulsars: 0.70 6 Pulsars: 0.40	8 Pulsars: 0.07 6 Pulsars: 0.04

Table 4
SIMULATION RESULTS FOR SIMULATED SPACECRAFT ORBITS

Integer Cycle Candidate Set Characteristics	GPS		DirecTV 2	
	8 Pulsars	6 Pulsars	8 Pulsars	6 Pulsars
# Initial Candidate Sets	138645	138645	467523	467523
# Above Sets Found Within Search Space Shell	32803	33199	35182	35523
# Sets Pass Double Difference Residual Test	27789	16883	29834	17851
# Sets Found Within Search Space Shell Using Single Difference	25569	15282	25973	14872
# Sets Pass Single Difference Residual Test	3	29	6	31
# Candidate Sets with Single Difference Residual < True Set	0	3	0	1
Magnitude of Position Error for Correct Candidate Set (km)	116	141	102	112

Using all eight pulsars and the simulated phase measurement error for this specific simulation run, the correct set of pulse candidates produce a position solution that have error magnitudes with respect to the true position of 116 km for the GPS orbit and 102 km for the DirecTV 2 orbit. Although these may appear to be large errors, the vehicle was initially assumed to exist at the center of Earth at the start of each process, thus the error in position has actually been significantly improved. The position error is dominated by the phase bias error introduced within the simulation. In an operational system, all attempts should be made to reduce this effect.

For various applications, the position solution produced by this method may be sufficient for the vehicle to complete its mission. For those applications that require additional accuracy, several options could be pursued. The methods described above could be used within an iterative process to yield improved solutions. Once the initial correct cycle set is determined, the process of creating pulse phase measurements could be recomputed using the new estimated position solution. This would reduce the phase measurement errors further and would produce improved range estimates. These new range estimates would consequently produce a position solution with greater accuracy. Iterative processes such as these would help produce solutions with sufficient accuracy for most applications. Alternatively, the estimated solution produced by this absolute position determination process could be utilized as the initial conditions for a recursive estimation process incorporating an orbit propagator [9, 13].

Future investigations are planned to further evaluate and enhance the techniques described here. This includes methods to improve the overall position accuracy from the algorithms, and identifying and removing false candidate sets. Additional X-ray sources are to be evaluated for their potential within the system. Further relative navigation experiments between multiple vehicles will also be conducted.

CONCLUSION

The algorithms and results presented here demonstrate the potential of using differenced phase measurements from variable celestial sources to compute spacecraft position. By determining the correct phase cycle set for the observed pulses from a set of pulsars, the range estimates between a reference location and the spacecraft can be computed for each observation. The several techniques discussed are designed to select the correct cycle set from a group of candidate sets. Combining the range estimates and the line-of-sight direction to each pulsar provides an approach to determine the full three-dimensional absolute position within an inertial coordinate system. The accuracy of the position solution depends on the error of each phase measurement. Autonomous simulated position error estimates for Earth-orbiting spacecraft are on the order of 10's km without any *a priori* knowledge of the vehicle's position vector. The techniques reported here require simultaneous measurements from several sources; although current day design concepts of variable celestial X-ray source-based spacecraft navigation observe each source sequentially; future systems may have the capability of multiple simultaneous measurements making these techniques feasible and eventually operational.

ACKNOWLEDGEMENT

The authors would like to thank the Metropolitan Washington DC Chapter of the Achievement Rewards for College Scientists (ARCS) Foundation and the Gustave J. Hokenson Fellowship of the Aerospace Engineering Department of the University of Maryland for a majority of the sponsorship for this research. They would like to thank the X-ray/UV Astrophysics and Applications Section at the Naval Research Laboratory, specifically Kent Wood, Paul Ray, and Michael Wolff for their assistance in pulsar characterization. Also, much appreciation goes to the entire DARPA X-ray Navigation and Autonomous Position Verification (XNAV) team, including specifically Dan Jablonski, John Goldsten, and Kenneth Nelson of the Johns Hopkins University Applied Physics Laboratory.

REFERENCES

1. Thornton, C. L., and Border, J. S., *Radiometric Tracking Techniques for Deep Space Navigation*, John Wiley & Sons, Hoboken, NJ, 2003.
2. Battin, R. H., *An Introduction to the Mathematics and Methods of Astrodynamics*, Revised ed., American Institute of Aeronautics and Astronautics, Washington, DC, 1999.
3. Parkinson, B. W., and Spilker, J. J. J. Eds., *Global Positioning System: Theory and Applications, Volume I*. American Institute of Aeronautics and Astronautics, Washington, DC, 1996.
4. Parkinson, B. W., and Spilker, J. J. J. Eds., *Global Positioning System: Theory and Applications, Volume II*. American Institute of Aeronautics and Astronautics, Washington, DC, 1996.
5. Downs, G. S., "Interplanetary Navigation Using Pulsating Radio Sources," *NASA Technical Reports N74-34150*, 1974, pp. 1-12.
6. Chester, T. J., and Butman, S. A., "Navigation Using X-ray Pulsars," *NASA Technical Reports N81-27129*, 1981, pp. 22-25.
7. Wood, K. S., "Navigation Studies Utilizing The NRL-801 Experiment and the ARGOS Satellite," *Small Satellite Technology and Applications III*, Ed. B. J. Horais, International Society of Optical Engineering (SPIE) Proceedings, Vol. 1940, 1993, pp. 105-116.

8. Hanson, J. E., "Principles of X-ray Navigation," Doctoral Dissertation, Stanford University, 1996, URL: http://il.proquest.com/products_umi/dissertations/.
9. Sheikh, S. I., "The Use of Variable Celestial X-ray Sources for Spacecraft Navigation," Ph.D. Dissertation, University of Maryland, 2005, URL: https://drum.umd.edu/dspace/handle/1903/2856.
10. Sheikh, S. I., Pines, D. J., Wood, K. S., Ray, P. S., Lovellette, M. N., and Wolff, M. T., "Spacecraft Navigation Using X-ray Pulsars," *Journal of Guidance, Control, and Dynamics*, Vol. 29, No. 1, 2006.
11. Sala, J., Urruela, A., Villares, X., Estalella, R., and Paredes, J. M., "Feasibility Study for a Spacecraft Navigation System relying on Pulsar Timing Information," European Space Agency Advanced Concepts Team, ARIADNA Study 03/4202, 23 June 2004.
12. Woodfork, D. W., "The Use of X-ray Pulsars for Aiding GPS Satellite Orbit Determination," Master of Science Thesis, Air Force Institute of Technology, 2005, URL: http://www.afit.edu.
13. Sheikh, S. I., and Pines, D. J., "Recursive Estimation of Spacecraft Position Using X-ray Pulsar Time of Arrival Measurements," *ION 61st Annual Meeting*, Institute of Navigation, Boston MA, 27-29 June 2005.
14. Manchester, R. N., and Taylor, J. H., *Pulsars*, W.H. Freeman and Company, San Francisco CA, 1977.
15. Lyne, A. G., and Graham-Smith, F., *Pulsar Astronomy*, Cambridge University Press, Cambridge UK, 1998.
16. Hewish, A., Bell, S. J., Pilkington, J. D., Scott, P. F., and Collins, R. A., "Observation of a Rapidly Pulsating Radio Source," *Nature*, Vol. 217, 1968, pp. 709-713.
17. Charles, P. A., and Seward, F. D., *Exploring the X-ray Universe*, Cambridge University Press, Cambridge UK, 1995.
18. Hellings, R. W., "Relativistic Effects in Astronomical Timing Measurements," *Astronomical Journal*, Vol. 91, 1986, pp. 650-659.
19. Bar-David, I., "Communication under the Poisson Regime," *IEEE Transactions on Information Theory*, Vol. 15, No. 1, 1969, pp. 31-37.
20. Kay, S. M., *Fundamentals of Statistical Signal Processing: Estimation Theory*, Prentice Hall, New Jersey, 1993.
21. Possenti, A., Cerutti, R., Colpi, M., and Mereghetti, S., "Re-examining the X-ray versus spin-down luminosity correlation of rotation powered pulsars," *Astronomy and Astrophysics*, Vol. 387, 2002, pp. 993-1002.
22. Nicastro, L., Cusumano, G., Löhmer, O., Kramer, M., Kuiper, L., Hermsen, W., Mineo, T., and Becker, W., "BeppoSAX Observation of PSR B1937+21," *Astronomy and Astrophysics*, Vol. 413, 2004, pp. 1065-1072.
23. Becker, W., and Trümper, J., "The X-ray luminosity of rotation-powered neutron stars," *Astronomy and Astrophysics*, Vol. 326, 1997, pp. 682-691.
24. Chakrabarty, D., and Morgan, E. H., "The two-hour orbit of a binary millisecond X-ray pulsar," *Nature*, Vol. 394, 1998, pp. 346-348.
25. Wijnands, R., "An XMM-Newton Observation during the 2000 Outburst of SAX J1808.4-3658," *Astrophysical Journal*, Vol. 588, 2003, pp. 425-429.
26. Strohmayer, T. E., Markwardt, C. B., Swank, J. H., and in't Zand, J., "X-Ray Bursts from the Accreting Millisecond Pulsar XTE J1814-338," *Astrophysical Journal*, Vol. 596, 2003, pp. L67-L70.
27. Abidin, H., "On the Construction of the Ambiguity Search Space for On-The-Fly," *Journal of the Institute of Navigation*, Vol. 40, No. 3, 1993, pp. 321-338.
28. Chlohessy, W. H., and Wiltshire, R. S., "Terminal Guidance System for Satellite Rendezvous," *Journal of Aerospace Sciences*, Vol. 27, No. 9, 1960, pp. 653-658, 674.
29. Kelso, T. S., "NORAD Two-Line Element Sets Historical Archives," [online database], Celestrak, URL: http://www.celestrak.com/NORAD/archives/request.asp [cited 22 December 2004].
30. Hoots, F. R., and Roehrich, R. L., "Spacetrack Report No. 3, Model for Propagation of NORAD Element Sets," Department of Defense, Defense Documentation Center, December 1980.